Exciton relaxation and coupling dynamics in a GaAs/$Al_xGa_{1-x}As$ quantum well and quantum dot ensemble

G. Moody,[1,2] M. E. Siemens,[1,*] A. D. Bristow,[1,†] X. Dai,[1,‡] A. S. Bracker,[3] D. Gammon,[3] and S. T. Cundiff[1,2,§]

[1]*JILA, University of Colorado and National Institute of Standards and Technology, Boulder, Colorado 80309-0440, USA*

[2]*Department of Physics, University of Colorado, Boulder, Colorado 80309-0390, USA*

[3]*Naval Research Laboratory, Washington, District of Columbia 20375, USA*

(Received 16 December 2010; revised manuscript received 22 March 2011; published 27 June 2011)

Exciton inter- and intra-actions in a GaAs/AlGaAs quantum well (QW) and quantum dot (QD) ensemble are studied using optical two-dimensional Fourier transform spectroscopy. We measure population dynamics for times up to 300 ps and temperatures up to 50 K and observe biexponential decay for both QW and QD excitons, strong QW → QD relaxation, and weak QD → QW activation. The population dynamics are modeled using a system of rate equations that incorporate radiative and nonradiative decay, coupling between bright and dark exciton states, and QW ↔ QD coupling. The fast decay rates are attributed to exciton-bound hole spin flips between optically active and inactive states and are similar for the QW and QDs, indicating excitons are weakly localized in the QDs. The QW → QD relaxation rate increases with temperature, and QD → QW excitation is observed at temperatures $\geqslant$35 K.

DOI: 10.1103/PhysRevB.83.245316 PACS number(s): 73.63.Kv, 73.63.Hs, 78.47.nj

I. INTRODUCTION

The nature of exciton and free carrier transfer phenomena in low-dimensional semiconductor heterostructures has been the focus of intense research, driven by an interest in novel physical properties emerging from increased confinement of the electronic wave function and continued development of fast and efficient optoelectronic devices.[1–3] Of particular interest in recent years has been carrier transfer between quantum dot (QD) states and a reservoir, such as a quantum well (QW) or wetting layer, through capture, thermal escape, and Auger scattering processes.[4–6] While many reports have focused primarily on free carrier dynamics, carrier transfer can also occur via QW ↔ QD coupling of excitons.[7,8] High-energy free carriers generated in the QW or barrier can relax to the QD ground state in a time ranging from picoseconds[9,10] to hundreds[11] of picoseconds, after which exciton-exciton, exciton-carrier, and exciton-phonon interactions must be considered when the thermal energy is less than the exciton binding energy.

Photoluminescence (PL) spectroscopies can be used to study transfer phenomena; however, the nonresonant generation of free carriers strongly influences the exciton dynamics. Nonlinear experiments, such as pump-probe or transient four-wave mixing (TFWM) techniques, can overcome this issue, although distinguishing between the numerous contributions to the signal can be difficult. In order to provide a clear picture of exciton population relaxation and transfer dynamics, resonant measurements that clearly separate the relevant relaxation and excitation paths are desired. In this work, inter- and intra-actions of QW and QD heavy-hole excitons are simultaneously resolved in an intrinsic GaAs/AlGaAs nanostructure using two-dimensional Fourier transform spectroscopy (2DFTS). 2DFTS is based on three-pulse TFWM with the enhancement of interferometric stabilization of the excitation pulse delays, which allows the signal to be unfolded onto two frequency dimensions.[12] Two-dimensional (2D) spectra are recorded for different fixed delays between the second and third excitation pulses, during which time incoherent population dynamics can be studied. Population decay and transfer are fit with exponential functions, and the fitted rates are used in a system of rate equations to provide insight into the primary decay and coupling mechanisms. Results reveal fast population decay within 10 ps of excitation, followed by a slow decay on the order of 100 ps. During this time, significant QW ↔ QD population transfer is observed as cross peaks in the 2D spectra.

II. SAMPLE AND EXPERIMENTAL TECHNIQUE

Transmission measurements are performed on a single GaAs/$Al_{0.3}Ga_{0.7}As$ QW, 4.2-nm thick, epitaxially grown on a GaAs (100) substrate. After growth, the substrate was removed by selective etching. An epitaxial growth interruption wait time on the order of tens of seconds results in monolayer width fluctuations in the QW thickness, which form islandlike features. Excitons in these islands are localized and confined by ≈10 meV in the lateral dimensions by the monolayer width difference in the QW. For this reason, these islands provide three-dimensional confinement and are known as interfacial QDs.[13] The amount of confinement is small compared to self-assembled QDs and is only strong enough to weakly localize the excitons.

Upon optical excitation with linearly polarized light, delocalized excitons are created in the QW and localized excitons are created simultaneously in the QD ensemble. These excitons are in the $J_Z = |\pm 1\rangle$ optically active bright states, shown in the energy level diagram in Fig. 1. Variations in the QD lateral dimensions inhomogeneously broadens the QD ensemble spectrum, while the QW spectrum is inhomogeneously broadened due to wave-function averaging over high-frequency width fluctuations that are too small for exciton localization. A GaAs/AlGaAs heterostructure is a model system to study QW ↔ QD coupling because of the defect-free growth process and large oscillator strength.[14,15] Furthermore, the small energy shift separating the QW and

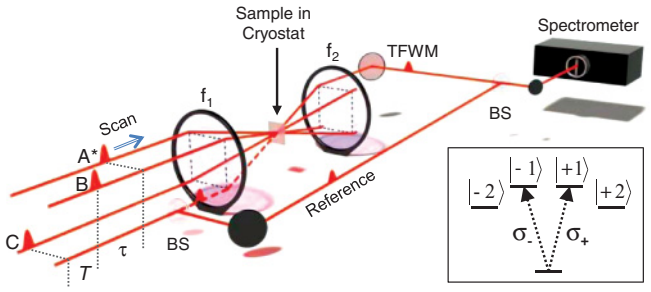

FIG. 1. (Color online) Schematic diagram of the optical 2DFTS experimental setup. Notation: f_i: lens; BS: beam splitter. Inset: energy level scheme relevant for the QW and QD heavy-hole excitons. Upon excitation by linearly polarized light, excitons are created in the $|\pm 1\rangle$ bright states.

QD excitons allows for simultaneous resonant excitation of both exciton populations within the laser bandwidth.

A schematic diagram of the experimental setup is shown in Fig. 1. The experiment is performed using a mode-locked Ti:sapphire laser generating 100 fs pulses at a repetition rate of 76 MHz. We tune the spectrum to be centered over the QD distribution for all temperatures, shown in the lower-left panel of Fig. 2 for 35 K. A phase-stabilized interferometer splits the pulses into four copies propagating in the box geometry,[16] collinearly polarized along the [110] crystal axis. Three of the pulses are focused onto the sample

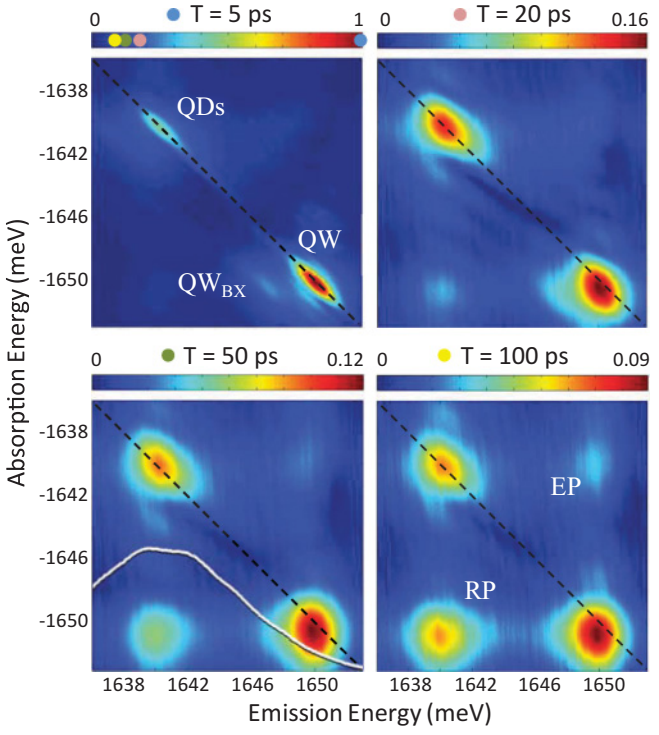

FIG. 2. (Color) QW exciton (QW), QW biexciton (QW_{BX}), QD exciton ensemble (QDs), QW → QD relaxation peak (RP), and QD → QW excitation peak (EP) are observed in the 2D amplitude spectra for increasing T. The temperature is fixed at 35 K. Each spectrum is normalized to the QW peak, and the amplitudes are marked on the $T = 5$ ps color bar. The laser spectrum is represented by the solid white line on the $T = 50$ ps 2D spectrum.

with a photon density of 3.0×10^{11} photons/(pulse cm^2), encompassing $\approx 10^5$ QDs, and the TFWM signal is emitted in the phase-matched direction $\mathbf{k}_s = -\mathbf{k}_a + \mathbf{k}_b + \mathbf{k}_c$. The signal is collinearly recombined with a phase-stabilized reference derived from the fourth pulse, and the heterodyned signal is spectrally resolved. The interferogram is recorded as the delay τ between the first two pulses, A^* and B, is stepped, while the delay T between pulses B and C is held fixed. The absorption axis of a 2D spectrum, $\hbar\omega_\tau$, is constructed by taking a Fourier transform with respect to τ, while the emission axis $\hbar\omega_t$ is generated by resolving the complex spectrum. The absorption axis is plotted as negative energy because the conjugate pulse A^* is incident on the sample first. The TFWM signal radiated from the QDs is weak and masked by pump light scattered in the phase-matched direction. Suppression of the pump scatter is achieved by cycling the phase of the excitation pulses during a 2D scan.[16,17]

III. EXPERIMENTAL RESULTS

Population dynamics can be studied by recording 2D spectra for different values of T because the signal phase does not evolve during this time delay. 2D amplitude spectra are shown in Fig. 2 for increasing T at 35 K. The spectra are normalized to the QW peak and the relative amplitudes are shown on the color bars. At short times, the inhomogeneity of the QW and QD excitons is seen as broadening along the diagonal (dashed line), and a weak QW biexciton is observed red shifted along the emission axis by the biexciton binding energy. As T increases, the QW and QD features decay and spectrally broaden. Cross peaks resulting from ground state bleaching and Raman coherences[18] are absent for $T = 0$; therefore, the appearance of cross peaks with increasing T indicates incoherent exciton population transport between the QW and QDs, which would be concealed in one-dimensional TFWM experiments. A relaxation peak (RP) appears at the absorption energy of the QW and emission energy of the QDs, revealing incoherent QW → QD exciton population relaxation and localization. Thermal activation of QD excitons is observed at long times as an excitation peak (EP) at the absorption energy of the QDs and emission energy of the QW. Both cross peaks are round, indicating equal coupling between all QW and QD states.

To quantify population relaxation and coupling, each peak is integrated within a region of ±3 meV from the peak center, encompassing >95% of the feature. A weak background is removed from each peak by subtracting the line integral of the enclosing region. Integrating each peak, as opposed to comparing excitons of specific energy, provides insight into the coupling mechanisms between the QW and QD exciton ensemble. Migration of QW excitons and transitions between QD states due to phonon activation, tunneling, or dipole-dipole interactions will not transfer excitons outside of the integrating region. Therefore, any contributions to the decay of the integrated signal are from radiative recombination, nonradiative scattering processes, spin relaxation to dark states, and QW ↔ QD coupling. The integrated RP values are divided by the QW + RP values in order to properly determine the degree to which excitons originating in the QW have relaxed to the QDs (similarly for the EP).

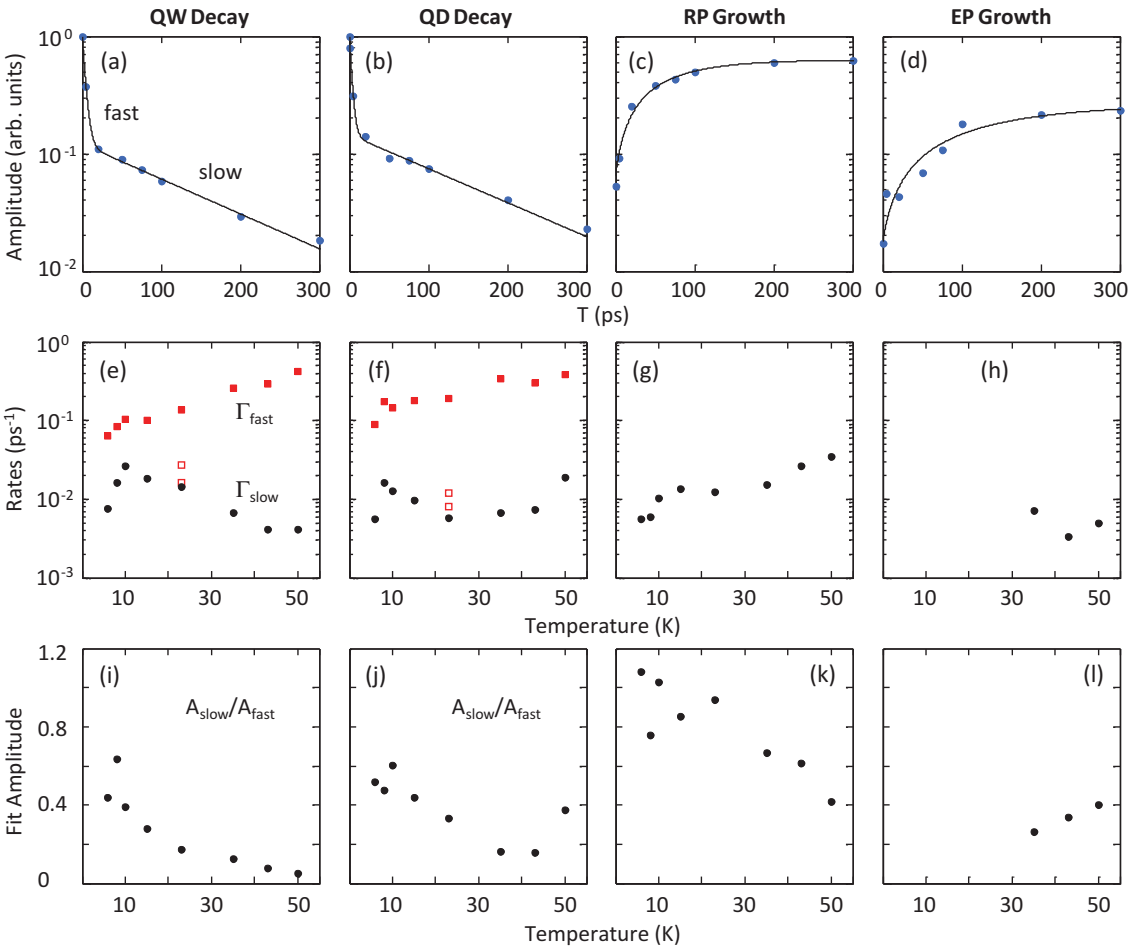

FIG. 3. (Color online) Biexponential decay of the integrated (a) QW and (b) QD peaks and the (c) RP and (d) EP growth with T at 35 K. Temperature dependence of rates extracted from the fits are shown for the (e) QW, (f) QDs, (g) RP, and (h) EP. The open squares in (e) and (f) represent the single exponential decay rate measured at higher photon densities, converging toward the slow decay rate with increasing density. Panels (a)–(h) are plotted on a logarithmic vertical scale. The final row shows the ratio of the slow and fast exponential decay fit amplitudes for the (i) QW and (j) QDs and the exponential growth fit amplitudes for the (k) RP and (l) EP. The EP is observed for temperatures $\geqslant$35 K.

The QW and QD peaks are characterized by a biexponential decay with T, shown using a logarithmic vertical scale in Figs. 3(a) and 3(b), respectively, for a temperature of 35 K. Values of $T > 200$ fs are used to avoid coherent transients and ambiguities in the time ordering from pulse overlap. The growth of the RP and EP is shown in Figs. 3(c) and 3(d), respectively, and is modeled using a fit function $\propto [1 - \exp(-\Gamma T)]$. Decay and growth rates are extracted from the fits and are shown as a function of temperature in Fig. 3 for the QW [Fig. 3(e)], QDs [Fig. 3(f)], RP [Fig. 3(g)], and EP [Fig. 3(h)]. The QW and QD fast and slow relaxation rates are on the order of 0.1 and 0.01 ps^{-1}, respectively. At temperatures $\leqslant$10 K, the RP growth rate is comparable to the QW and QD slow decay rates, while at higher temperatures, it becomes twice as fast. The EP is observed at temperatures $\geqslant$35 K, and its growth rate is $<$0.01 ps^{-1}. Observation of the EP at temperatures $<$50 K is in contrast to self-assembled QD systems with stronger confinement. In these systems, optical phonons play a significant role in the relaxation process, and wetting layer/barrier $\rightarrow$ QD relaxation rates from 0.01 to 0.1 ps^{-1} have been measured; [19,20] however, excitation out of the QDs occurs only at a much higher temperature because of the strong confinement.[21]

The temperature dependence of the ratio of the slow and fast decay fit amplitudes are shown in Figs. 3(i) and 3(j) for the QW and QDs, respectively, and for the RP and EP growth fit amplitudes in Figs. 3(k) and 3(l), respectively. The QW and QD amplitude ratios exhibit an overall decrease with temperature, indicating an enhancement of population decay within the first 10 ps. With increasing temperature, the RP amplitude decays from unity to $\approx\frac{1}{2}$, while the EP amplitude increases from zero to that of the RP at 50 K.

IV. MODEL

For an interpretation of the results, it is useful to consider the possible population relaxation and transfer paths illustrated in Fig. 4. In this model, elongation of the QDs along the [$\bar{1}$10] crystal axis resulting in fine-structure splitting of the linearly polarized exciton eigenstates[22] is ignored for reasons discussed in Sec. V. For simplicity, $\pm$ spin states are combined to give four exciton states. An exciton population is resonantly created

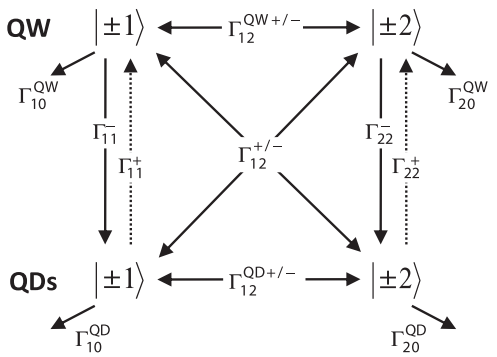

FIG. 4. Possible decay channels within and between QW and QD exciton spin states are highlighted. Transfer rates between QW and QD states are labeled as $\Gamma_{ij}^{+/-}$, where the + (–) corresponds to excitation (relaxation) and i (j) corresponds to the initial (final) state. Electron/hole spin flips transfer the exciton between the $|\pm1\rangle$ and $|\pm2\rangle$ states at a rate of $\Gamma_{12}^{QW+/-}$ for the QW and $\Gamma_{12}^{QD+/-}$ for the QDs. QW/QD population decay to the ground state, through radiative and nonradiative processes, occurs at a rate of $\Gamma_{i0}^{QW/QD}$, where i is either 1 or 2 depending on the exciton spin state.

in the bright $|\pm1\rangle$ QW and QD states and can decay through radiative recombination and nonradiative processes, such as scattering from defects or exciton-exciton Auger scattering. Alternatively, bright excitons can couple to the dark $|\pm2\rangle$ states through electron or hole spin flips. Reverse spin-flip processes also exist such that excitons may return from $|\pm2\rangle$ to $|\pm1\rangle$. In the limit that these processes are fast compared to recombination, a quasiequilibrium population distribution of the bright and dark states will form and the decay of this distribution is reflected in the slow decay rate of the QW and QD populations. It is limited by recombination and nonradiative scattering, slower spin-flip processes, and QW $\leftrightarrow$ QD coupling. QW excitons can relax directly to QD states through phonon scattering and emission or indirectly involving multiple spin flips. Cross coupling between QW and QD bright and dark states involves relaxation and a single electron or hole spin flip and occurs on a longer timescale compared to direct relaxation. Indirect coupling involving more than one path in Fig. 4 occurs at a rate that is a combination of the rates of each individual path, and the likelihood of population transfer along a given path decreases with the number of paths involved. Conversely, bright and dark QD excitons can be excited to the QW states along reverse paths of QW $\rightarrow$ QD relaxation.

We use a system of rate equations to model the QW–QD coupling dynamics we observe. A complete theoretical model is a significant undertaking; therefore, the goal of the proposed model is not to encompass all QW and QD intra-actions, but to connect the transfer phenomena we observe with coupling between the involved states. The model incorporates radiative and nonradiative decay, bright and dark state coupling, and relaxation or excitation between QW and QD states. Despite this simplification, reasonable agreement between the data and the model provides significant insight into the system dynamics. These mechanisms are demonstrated in Eqs. (1)–(4), where the exciton population in the QW is $N_{\pm i}^{QW}$ and in the QDs is $N_{\pm i}^{QD}$, $G_i^{QW/QD}$ is the number of available states defined as $(1 - N_{\pm i}^{QW/QD}/N_{max}^{QW/QD})$, and i is the spin state:

$$\dot{N}_{\pm1}^{QW} = -\left(\Gamma_{10}^{QW} + \Gamma_{12}^{QW-}G_2^{QW} + \Gamma_{11}^{-}G_1^{QD} + \Gamma_{12}^{-}G_2^{QD}\right)N_{\pm1}^{QW} + \left(\Gamma_{11}^{+}N_{\pm1}^{QD} + \Gamma_{12}^{QW+}N_{\pm2}^{QW} + \Gamma_{12}^{+}N_{\pm2}^{QD}\right)G_1^{QW}, \quad (1)$$

$$\dot{N}_{\pm2}^{QW} = -\left(\Gamma_{20}^{QW} + \Gamma_{12}^{QW+}G_1^{QW} + \Gamma_{22}^{-}G_2^{QD} + \Gamma_{12}^{-}G_1^{QD}\right)N_{\pm2}^{QW} + \left(\Gamma_{22}^{+}N_{\pm2}^{QD} + \Gamma_{12}^{QW-}N_{\pm1}^{QW} + \Gamma_{12}^{+}N_{\pm1}^{QD}\right)G_2^{QW}, \quad (2)$$

$$\dot{N}_{\pm1}^{QD} = -\left(\Gamma_{10}^{QD} + \Gamma_{12}^{QD-}G_2^{QD} + \Gamma_{11}^{+}G_1^{QW} + \Gamma_{12}^{+}G_2^{QW}\right)N_{\pm1}^{QD} + \left(\Gamma_{11}^{-}N_{\pm1}^{QW} + \Gamma_{12}^{QD+}N_{\pm2}^{QD} + \Gamma_{12}^{-}N_{\pm2}^{QW}\right)G_1^{QD}, \quad (3)$$

$$\dot{N}_{\pm2}^{QD} = -\left(\Gamma_{20}^{QD} + \Gamma_{12}^{QD+}G_1^{QD} + \Gamma_{22}^{+}G_2^{QW} + \Gamma_{12}^{+}G_1^{QW}\right)N_{\pm2}^{QD} + \left(\Gamma_{22}^{-}N_{\pm2}^{QW} + \Gamma_{12}^{QD-}N_{\pm1}^{QD} + \Gamma_{12}^{-}N_{\pm1}^{QW}\right)G_2^{QD}. \quad (4)$$

The combined radiative recombination and nonradiative decay rates $\Gamma_{10}^{QW/QD}$ are the measured slow decay rates in Fig. 3; the bright-to-dark coupling rates $\Gamma_{12}^{QW/QD-}$ are the measured fast decay rates; Γ_{11}^{-} is related to the measured RP growth rate; Γ_{11}^{+} is related to the measured EP growth rate; and the cross-coupling rates $\Gamma_{12}^{+/-}$ equal $\Gamma_{11}^{+/-}$ $\Gamma_{12}^{QW/QD+/-}$. The sum of the rates contributing to the RP and EP in the model are set equal to the measured growth rates of the peaks. Dipole selection rules prevent radiative decay of the dark states; thus, $\Gamma_{20}^{QW/QD}$ reflects nonradiative decay processes and is fixed to be an order of magnitude less than $\Gamma_{10}^{QW/QD}$ in order to best match the population at long times. QW–QD coupling rates $\Gamma_{22}^{+/-}$ are set equal to $\Gamma_{11}^{+/-}$. The dark-to-bright spin-flip rates Γ_{12}^{QW+} and Γ_{12}^{QD+} are adjusted between 0.035 and 0.045 ps^{-1} and 0.065 and 0.07 ps^{-1}, respectively, in order to match the amount of initial population decay at short time. Because a low photon density is used, the exciton states are expected to be far from saturation, and $N_{max}^{QW/QD}$ is fixed at an order of magnitude larger than the initial population in each state. The system of rate equations is solved, and the solutions (solid lines) are shown in Fig. 5 with the measured population (points) at 35 K. The free parameters in the equations are the dark state decay rates $\Gamma_{20}^{QW/QD}$ and dark-to-bright state spin-flip rates $\Gamma_{12}^{QW/QD+}$. The rates are consistent with detailed balance at the highest temperature, when QW $\leftrightarrow$ QD coupling is significant and the system is in a quasiequilibrium state. Departure from detailed balance at low temperature is not surprising because the exciton populations decay before equilibrium is reached.

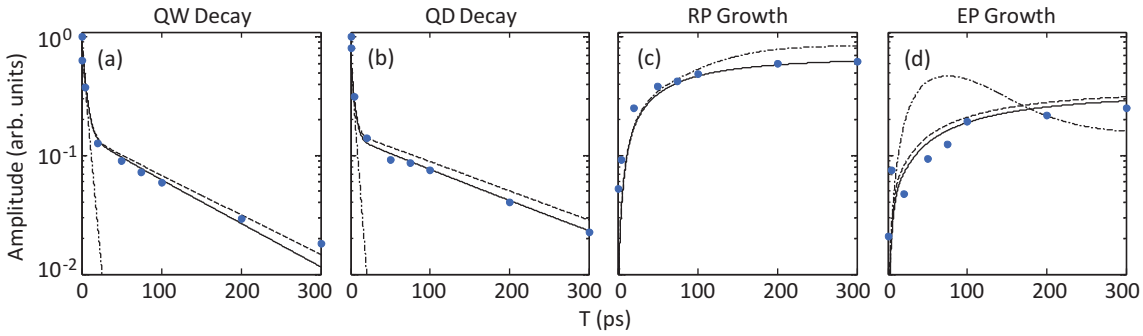

FIG. 5. (Color online) Measured (points) and calculated (solid lines) populations of the (a) QW, (b) QDs, (c) RP, and (d) EP obtained by solving the system of rate equations [Eqs. (1)–(4)]. Rates used in the equations are obtained from exponential decay and growth fits to the data displayed in Fig. 3, except for $\Gamma_{12}^{QW/QD+}$ and $\Gamma_{20}^{QW/QD}$, which are adjusted to obtain best agreement between the model and data. The calculated populations with $\Gamma_{20}^{QW/QD}$ (dashed line) and $\Gamma_{12}^{QW/QD+}$ (dashed-dotted line) equal to zero are also shown.

V. DISCUSSION

The agreement between the rate equation solutions and the measured populations shown in Fig. 5 provides insight into the primary decay and coupling mechanisms for the QW–QD system. To obtain a biexponential QW and QD population decay, a transfer mechanism is required such that a quasiequilibrium population distribution is created between multiple states. It is well established that QW exciton-bound hole spin relaxation occurs within picoseconds due to the strong electron-hole exchange interaction,[23] and we attribute the QW fast decay rate to this mechanism. Excitons initially in the $|\pm 1\rangle$ bright states hole spin flip to the $|\mp 2\rangle$ dark states, after which they can nonradiatively decay or spin flip back to the bright states. The formation of a quasiequilibrium distribution between these two states is indicated by the onset of the slow exponential decay.

Relaxation of excitons confined in QDs is expected to occur more slowly than in QWs due to suppression of effective momentum-scattering mechanisms.[24,25] However, experiments have found that the mechanisms responsible for fast spin relaxation in QWs are not entirely inhibited[26] for excitons weakly localized in interfacial GaAs QDs.[27,28] Coupling between linearly polarized QD eigenstates through exciton spin relaxation can contribute to population decay, but this relaxation process occurs on a time scale an order of magnitude longer than the fast decay we observe[26] and is combined with other slow processes in the rate Γ_{10}^{QD}. These results suggest that the same exciton-bound hole spin-flip mechanisms in the QW are prevalent in the QDs, and we include this coupling through terms with rate Γ_{12}^{QD-} in the model. The increase of the QW and QD fast decay rates with temperature is consistent with previous studies on hole spin lifetimes in narrow GaAs-based QWs.[29,30]

The QW and QD populations exhibit a single exponential decay as the photon density is increased, and the decay rates converge toward the slow decay rates, shown as open squares in Figs. 3(e) and 3(f), respectively, for 23 K. This behavior can be modeled by setting the maximum number of states $N_{max}^{QW/QD}$ equal to the initial population in the bright states, which represents saturation of the optical transition by decreasing the number of available states $G_i^{QW/QD}$. While exciton-exciton Auger scattering increases with excitation density, modeling this mechanism by including terms $\propto \Gamma_{Auger} N_i^{QW/QD}$ has an opposite effect—the QW and QD population decay rates converge toward a single fast decay rate. Therefore, the observed biexponential decay suggests that exciton-exciton Auger scattering is weak or negligible and that the experiment is performed in a low photon density regime such that the number of available states greatly exceeds the initial population.

The ratio of slow and fast exponential fit amplitudes for the QW and QDs, shown in Figs. 3(i) and 3(j), respectively, are $\approx \frac{1}{2}$ below 10 K and then decrease with temperature. For collinear polarization, both excited-state population and ground-state depletion terms equally contribute to the TFWM signal, and only the excited-state population term can decay through hole spin relaxation to the dark state. Consequently, in the limit of slow exciton spin relaxation and neglecting the biexciton state, the amplitude ratio to which the initial QW and QD populations decay is expected to be $\approx \frac{1}{2}$. The decrease of the amplitude ratio with temperature indicates that additional mechanisms beyond our model influence the initial population decay. One possible mechanism could be scattering of excitons to nonradiative large momentum states through exciton-acoustic phonon interactions, and this mechanism has been shown to primarily affect the initial population decay of resonantly excited QW excitons in PL experiments.[31] We can account for this decay below $\frac{1}{2}$ in the model by adjusting Γ_{12}^{QW+} and Γ_{12}^{QD+} for all temperatures to match the initial population decay. This is justified because the dominant contribution to the RP and EP in the model is direct bright-to-bright QW $\leftrightarrow$ QD coupling, which depends on the number of QW and QD excitons in the bright states irrespective of the mechanisms governing their population or decay. The dashed-dotted line in Fig. 5 shows the populations when $\Gamma_{12}^{QW/QD+}$ equals zero and emphasizes the significance of the bright-to-dark transfer mechanism for obtaining a QW and QD biexponential decay and for matching the growth rates and amplitudes of the RP and EP.

At long T, the QW and QD populations depend primarily on the slow decay rates, which are fixed from measurements, and on relaxation from the QW and excitation out of the QDs,

which is shown to occur at a rate comparable to the slow decay rate in Figs. 3(g) and 3(h), respectively. In the model, the dark state slow decay rates are set to an order of magnitude slower than those for the bright states because the dark states decay nonradiatively. When these rates are set equal to zero (dashed line in Fig. 5), the QW and QD slow decay rates decrease, the RP is essentially unaffected, and the EP growth rate and amplitude increase. While QW $\leftrightarrow$ QD cross coupling between bright and dark states contributes to the decay of the QW and QD populations, a cross peak will only be observable when the final state is bright.

Observation of the RP and EP indicates significant QW $\leftrightarrow$ QD relaxation and excitation to the $|\pm 1\rangle$ states. Although the QW can couple to the QDs through each path in Fig. 4, the likelihood of a given process occurring decreases with an increasing number of involved paths. The most likely QW $\rightarrow$ QD exciton transfer path is directly between the QW and QD $|\pm 1\rangle$ states, which requires acoustic phonon emission for energy conservation. A possible exciton-phonon coupling mechanism is the following: zero-momentum excitons initially delocalized in the QW scatter from the phonon population, acquiring a nonzero momentum. The exciton then relaxes into a QD state while emitting one or multiple acoustic phonons of the appropriate energy and momentum. Because excitons localized in the QDs have a momentum distribution about $\mathbf{K} = 0$, QW excitons with zero initial momentum can also relax to a QD state while emitting acoustic phonons to lose 10 meV of energy corresponding to the QW–QD energy separation. Additionally, the 10 meV between the QW and QDs can be overcome through a cascaded phonon relaxation process involving dark excited QD states.[19,32,33] With increasing temperature, the RP exponential fit amplitude decreases from $\approx$unity at 6 K to 0.4 at 50 K. Although the relaxation rate increases with temperature, the process itself becomes inhibited and only $\approx$half of the initial QW population relaxes to the bright QD states; the decay in amplitude is attributed to an increase in the relaxation rate to the dark QD states. As the hole spin-flip rate $\Gamma_{12}^{\mathrm{QW}-}$ increases with temperature, the cross-coupling relaxation rate also increases such that at high temperature QW excitons in the bright states decay equally to the bright and dark QD states.

Generation of the EP through QD $\rightarrow$ QW activation involves similar paths as the relaxation process in Fig. 4; however, the physical mechanisms are different. Excitons in the QDs must overcome the lateral confinement energy and be excited to a QW state. This phonon-activated process requires one or multiple acoustic phonons with at least $\approx$10 meV total energy, as opposed to the exciton-phonon scattering event during relaxation. The EP is observed for temperatures $\geqslant$35 K, at which a significant acoustic phonon population with energy $\geqslant$10 meV exists. While a multiphonon activation process is possible, the lack of an EP at lower temperatures indicates that QD $\rightarrow$ QW activation is much more likely to involve a single phonon. The EP amplitude increases from zero below 35 K to 0.4 at 50 K. Because the mechanisms contributing to growth of the EP are different than those for the RP, a definite conclusion regarding the behavior of the EP amplitude cannot be made. Nonetheless, the results suggest that the excitation process becomes more efficient as the number of phonons with the required energy to activate QD excitons to the QW states increases with temperature. As in the QW, the increase in the hole spin-flip rate $\Gamma_{12}^{\mathrm{QD}-}$ with temperature suggests that at higher temperature, the amplitude will approach $\approx\frac{1}{2}$ because the QD excitons will be activated to either QW bright or dark state equally likely.

Best agreement between the model and the data is obtained when including cross coupling at rates $\Gamma_{12}^{+/-}$ and QW $\leftrightarrow$ QD dark state coupling at rates $\Gamma_{22}^{+/-}$, such that the measured rates $\Gamma_{\mathrm{RP/EP}}$ are equal to the sum of the rates contributing to their growth. Indirect contributions to the RP and EP involve at least two spin flips and a relaxation or excitation mechanism, and they influence the solutions of the system of rate equations significantly less than the direct coupling path; however, their inclusion results in better agreement between the model and data by slightly increasing the amplitude and growth rate of the RP and EP and increasing the slow decay rate of the QW and QDs. The exciton-phonon coupling mechanisms relevant for QW $\leftrightarrow$ QD transfer in combination with the thermal behavior of both QW and QD decay rates are reflected in the temperature dependence of the RP and EP growth rates shown in Figs. 3(g) and 3(h), respectively.

VI. SUMMARY

Exciton QW $\leftrightarrow$ QD coupling through population relaxation and excitation has been studied in a GaAs/AlGaAs heterostructure using two-dimensional Fourier transform spectroscopy. This technique allows the simultaneous observation of population decay and coupling dynamics of excitons resonantly created in bright QW and QD states. QW and QD exciton populations were fit with a biexponential decay, and growth of the EP and RP were fit with an asymptotic exponential function. Rates and amplitudes were recorded as the temperature was increased from 6 to 50 K. A system of rate equations was used to model the dynamics and agreement with the measurements was obtained.

These results indicate that excitons initially in the bright states create a quasiequilibrium distribution with the dark states through hole spin flipping, revealed by the fast initial population decay of the QW and QD excitons. The decay of this distribution is reflected in the slow decay rate of the QW and QD populations through radiative and nonradiative decay, slower spin-flipping mechanisms, and QW $\leftrightarrow$ QD coupling. Strong coupling between QW and QD excitons exists through QW $\rightarrow$ QD relaxation processes, while weak QD $\rightarrow$ QW excitation occurs at temperatures $\geqslant$35 K.

ACKNOWLEDGMENTS

This work was supported by the National Science Foundation, the US Department of Energy, and the Chemical Sciences, Geosciences, and Biosciences Division, Office of Basic Energy Sciences. MES acknowledges funding from the National Academy of Sciences/National Research Council.

*Present address: Department of Physics and Astronomy, University of Denver, Denver, CO 80208-6900, USA.
†Present address: Department of Physics, West Virginia University, Morgantown, WV 26506-6315, USA.
‡Present address: Department of Physics, Tsinghua University, 100084 Beijing, China.
§cundiff@jila.colorado.edu

[1] S. Fafard, K. Hinzer, S. Raymond, M. Dion, J. McCaffrey, Y. Feng, and S. Charbonneau, Science **274**, 1350 (1996).
[2] D. L. Huffaker, G. Park, Z. Zou, O. B. Shchekin, and D. G. Deppe, Appl. Phys. Lett. **73**, 2564 (1998).
[3] S. Raghavan, D. Forman, P. Hill, N. R. Weisse-Bernstein, G. von Winckel, P. Rotella, S. Krishna, S. W. Kennerly, and J. W. Little, J. Appl. Phys. **96**, 1036 (2004).
[4] M. Braskén, M. Lindberg, M. Sopanen, H. Lipsanen, and J. Tulkki, Phys. Rev. B **58**, 15993 (1998).
[5] X. Mu, Y. J. Ding, Z. Wang, and G. J. Salamo, Laser Phys. Lett. **2**, 538 (2005).
[6] S.-W. Chang, S.-L. Chuang, and N. Holonyak Jr., Phys. Rev. B **70**, 125312 (2004).
[7] Yu. I. Mazur, B. L. Liang, Zh. M. Wang, D. Guzun, G. J. Salamo, Z. Ya. Zhuchenko, and G. G. Tarasov, Appl. Phys. Lett. **89**, 151914 (2006).
[8] T. V. Torchynska, J. L. Casas Espinola, L. V. Borkovska, S. Ostapenko, M. Dybiec, O. Polupan, N. O. Korsunska, A. Stintz, P. G. Eliseev, and K. J. Malloy, J. Appl. Phys. **101**, 024323 (2007).
[9] J. Feldmann, S. T. Cundiff, M. Arzberger, G. Böhm, and G. Abstreiter, J. Appl. Phys. **89**, 1180 (2001).
[10] L. Zhang, T. F. Boggess, D. G. Deppe, D. L. Huffaker, O. B. Shchekin, and C. Cao, Appl. Phys. Lett. **76**, 1222 (2000).
[11] F. Adler, M. Geiger, A. Bauknecht, F. Scholz, H. Schweizer, M. H. Pilkuhn, B. Ohnesorge, and A. Forchel, J. Appl. Phys. **80**, 4019 (1996).
[12] S. T. Cundiff, T. Zhang, A. D. Bristow, D. Karaiskaj, and X. Dai, Acc. Chem. Res. **42**, 1423 (2009).
[13] D. Gammon, E. S. Snow, B. V. Shanabrook, D. S. Katzer, and D. Park, Science **273**, 87 (1996).
[14] L. C. Andreani, G. Panzarini, and J.-M. Gérard, Phys. Rev. B **60**, 13276 (1999).
[15] J. R. Guest, T. H. Stievater, X. Li, J. Cheng, D. G. Steel, D. Gammon, D. S. Katzer, D. Park, C. Ell, A. Thränhardt, G. Khitrova, and H. M. Gibbs, Phys. Rev. B **65**, 241310(R) (2002).
[16] A. D. Bristow, D. Karaiskaj, X. Dai, T. Zhang, C. Carlsson, K. R. Hagen, R. Jimenez, and S. T. Cundiff, Rev. Sci. Instrum. **80**, 073108 (2009).
[17] R. R. Ernst, G. Bodenhausen, and A. Wokaun, *Principles of Nuclear Magnetic Resonance in One and Two Dimensions* (Clarendon, Oxford, 1988).
[18] L. Yang, T. Zhang, A. D. Bristow, S. T. Cundiff, and S. Mukamel, J. Chem. Phys. **129**, 234711 (2008).
[19] B. Ohnesorge, M. Albrecht, J. Oshinowo, A. Forchel, and Y. Arakawa, Phys. Rev. B **54**, 11532 (1996).
[20] R. Heitz, M. Veit, N. N. Ledentsov, A. Hoffmann, D. Bimberg, V. M. Ustinov, P. S. Kop'ev, and Zh. I. Alferov, Phys. Rev. B **56**, 10435 (1997).
[21] T. V. Torchynska, Superlattices Microstruct. **45**, 349 (2009).
[22] D. Gammon, E. S. Snow, B. V. Shanabrook, D. S. Katzer, and D. Park, Phys. Rev. Lett. **76**, 3005 (1996).
[23] M. Z. Maialle, E. A. de Andrada e Silva, and L. J. Sham, Phys. Rev. B **47**, 15776 (1993).
[24] T. Takagahara, J. Lumin. **87**, 308 (2000).
[25] A. V. Khaetskii and Yu. V. Nazarov, Physica E **6**, 470 (2000).
[26] T. H. Stievater, X. Li, T. Cubel, D. G. Steel, D. Gammon, D. S. Katzer, and D. Park, Appl. Phys. Lett. **81**, 4251 (2002).
[27] G. Moody, M. E. Siemens, A. D. Bristow, X. Dai, D. Karaiskaj, A. S. Bracker, D. Gammon, and S. T. Cundiff, Phys. Rev. B **83**, 115324 (2011).
[28] S. T. Cundiff, A. D. Bristow, M. Siemens, H. Li, G. Moody, D. Karaiskaj, X. Dai, and T. Zhang, IEEE J. Sel. Top. Quantum Electron (to appear).
[29] S. Adachi, T. Miyashita, S. Takeyama, Y. Takagi, and A. Tackeuchi, J. Lumin. **72-74**, 307 (1997).
[30] R. Ferreira and G. Bastard, Europhys. Lett. **23**, 439 (1993).
[31] A. Vinattieri, J. Shah, T. C. Damen, D. S. Kim, L. N. Pfeiffer, M. Z. Maialle, and L. J. Sham, Phys. Rev. B **50**, 10868 (1994).
[32] V. Savona and W. Langbein, Phys. Rev. B **74**, 075311 (2006).
[33] R. Heitz, M. Grundmann, N. N. Ledentsov, L. Eckey, M. Veit, D. Bimberg, V. M. Ustinov, A. Yu. Egorov, A. E. Zhukov, P. S. Kop'ev, and Zh. I. Alferov, Appl. Phys. Lett. **68**, 361 (1995).